Macromolecules

pubs.acs.org/Macromolecules
Article

Design and Characterization of Thioester Networks with Adaptable and Enzymatically Degradable Cross-Links

Shivani Desai, Gautam V. Khare, Kristi S. Anseth, and Kelly M. Schultz*

Cite This: Macromolecules 2025, 58, 3872−3885
Read Online

ACCESS | Metrics & More | Article Recommendations | Supporting Information

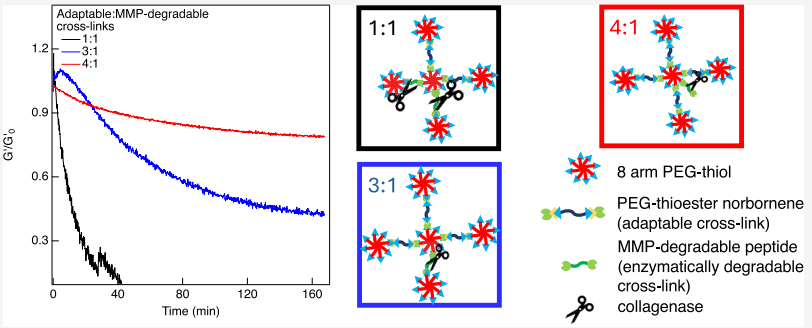

ABSTRACT: Viscoelastic properties of the extracellular matrix (ECM) impact cell processes including proliferation, spreading, and migration. During these basic cellular processes, cells remodel the ECM by secreting enzymes and applying cytoskeletal tension to the network. To design cell delivery platforms that mimic physical ECM properties, new designs incorporate viscoelasticity and moieties that enable cell-mediated network remodeling. In this work, we design and characterize networks with two different types of cross-links, covalent adaptable and enzymatically degradable. Our networks consist of 8-arm poly(ethylene glycol) (PEG)-thiol, PEG-thioester norbornene, and a norbornene functionalized matrix metalloproteinase (MMP)-degradable peptide, KKGPQG↓IWGQKK. We characterize three network compositions with a ratio of 1:1, 3:1, and 4:1 adaptable to MMP-degradable cross-links. We characterize network mechanical properties using bulk rheology. Using multiple particle tracking microrheology (MPT), we measure the evolving microstructure of the network during degradation. MPT measures Brownian motion of fluorescently labeled probe particles, which can be used to calculate rheological properties. Our results show that the elastic modulus increases with an increasing ratio of adaptable to MMP-degradable cross-links, and all networks have the same extent of stress relaxation. We then measure degradation of these networks by incubating in L-cysteine, which degrades only the adaptable cross-links by the thioester exchange reaction. We measure complete degradation of all three compositions using bulk rheology. Networks with 4:1 adaptable to MMP-degradable cross-links are the slowest to degrade and networks with 3:1 adaptable to MMP-degradable cross-links are the fastest to degrade. MPT measurements during degradation show networks with 1:1 and 4:1 adaptable to MMP-degradable cross-links rearrange multiple times before complete degradation. In networks with 3:1 adaptable to MMP-degradable cross-links, we measure fewer network rearrangements prior to degradation. Using time-cure superposition (TCS), we measure the network structure at the phase transition. Networks with 1:1 and 4:1 adaptable to MMP-degradable cross-links are elastic and tightly cross-linked and networks with 3:1 adaptable to MMP-degradable cross-links can range from elastic to open networks. The most open network structure, networks with 3:1 adaptable to MMP-degradable cross-links, degrade on the shortest time scale. We also measure ≥70% hMSC viability in each network after 3D encapsulation. In this work, we characterize different compositions of hybrid networks that incorporate both adaptable and enzymatically degradable cross-links. This work can enable design that specifies the mechanical properties and degradation behavior of the material to better mimic aspects of the native ECM.

INTRODUCTION

Cells reside in the extracellular matrix (ECM), which provides a dynamic viscoelastic environment. Mechanical properties of the ECM, including viscoelasticity and stiffness, impact basic cellular processes such as motility, proliferation, and differentiation.[1−4] During these basic cellular processes, cells are also constantly remodeling their microenvironment by secreting matrix metalloproteinases (MMPs). Previous work has shown that cell-mediated degradation and remodeling of microenvironments are essential to retain cellular function.[5−7] To use materials as cell delivery vehicles, scaffolds must

Received: February 20, 2025
Revised: March 28, 2025
Accepted: April 1, 2025
Published: April 8, 2025

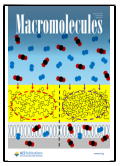

https://doi.org/10.1021/acs.macromol.5c00487
Macromolecules 2025, 58, 3872−3885

instruct cells after implantation, ideally using environmental cues that mimic aspects of the native ECM. Our work designs new scaffolds that use a combination of adaptable and enzymatically degradable cross-linkers to tune viscoelasticity and stiffness independently to mimic cell-engineered microenvironments.

Covalent adaptable networks (CANs), polymeric networks with adaptable cross-links, mimic the viscoelastic properties of the ECM.[8,9] In these materials, cross-links can be rearranged by the addition of external stimuli such as pH, shear, or temperature. The rearrangement of cross-links provides these networks with stress relaxation properties similar to the ECM and enables recovery of mechanical properties after being pushed out of equilibrium.[10,11] For cell delivery, these materials can protect encapsulated cells during injection by a syringe and the matrix can reform at the delivery site.[10,12,13] Different chemistries such as hydrazone,[14−17] boronic acid,[18,19] thioester,[20,21] and Diels−Alder[22] have been used to make CANs. The goal of this work is to design a synthetic matrix that mimics both the viscoelasticity and MMP-degradability of the ECM.

Hybrid networks with adaptable and MMP-degradable cross-links have been previously reported. Purcell et al. design hybrid hydrogels that reduce excess MMP activity after myocardial infarction.[12] These materials are hyaluronic acid (HA)-based networks with adaptable hydrazone and MMP-cleavable cross-links. Hydrazone cross-links are used to make the hydrogel injectable. Hybrid networks with permanent and MMP-degradable cross-links have also been reported as cell culture platforms. These materials are HA-based hybrid hydrogels with variable amounts of permanent and enzymatically degradable cross-links, which are used to encapsulate human salivary gland stem/progenitor cells (hS/PC).[23] They show that including MMP-degradability enhances the regenerative potential of hS/PCs while permanent cross-links prevent these hydrogels from completely degrading over 15 days. These materials have promise for advanced biological applications.

In this work, taking inspiration from the native ECM which is viscoelastic and can be remodeled by cell-secreted MMPs, we design and characterize networks that mimic these ECM properties. We design thioester CANs that consist of poly(ethylene glycol) (PEG)-thiol and PEG-thioester norbornene (PEG-TENB). These hydrogels are adaptable in nature due to a thioester exchange reaction. When excess thiol is present in the network, it forms a thiolate ion. Nucleophilic attack of the thiolate ion in the network cross-links results in a thioester exchange reaction that rearranges network cross-links. To make these hydrogels proteolytically degradable, we add a norbornene functionalized peptide, KKGPQG↓IWGQKK, which can be cleaved by cell-secreted MMPs. We modify a thioester CAN with 100% excess thiol that we have previously characterized.[13] We change the ratio of adaptable to MMP-degradable cross-links and hypothesize that these materials will retain the viscoelastic properties of thioester networks with 100% excess thiol. We use bulk rheology to characterize the mechanical properties of each network, including the storage modulus, G', and stress relaxation. We also characterize network degradation in L-cysteine or collagenase using bulk rheology. We then characterize the evolving rheology and structure of these networks during degradation in L-cysteine using multiple particle tracking microrheology (MPT). MPT has been used to characterize structural changes in materials during degradation and gelation in various networks.[24−31] By characterizing the structural evolution of these scaffolds, we can design new materials that precisely control the extent of scaffold degradation and temporal viscoelastic properties of the network, both of which can impact and direct encapsulated cellular processes. We also 3D encapsulate human mesenchymal stem cells (hMSCs) and measure cell viability is ≥70% in all hybrid networks. Overall, this work designs and characterizes new hydrogel platforms that mimic ECM viscoelasticity and enable cell-mediated remodeling.

MATERIALS AND METHODS

Hydrogel Scaffold Design and Compositions. In this work, we design three different compositions of thioester networks. These hydrogels are designed using 8-arm PEG-thiol (M_n = 20,000 g/mol, f = 8, where f is the number of functional groups, JenKem Technology USA Inc.), PEG-thioester norbornene (PEG-TENB, M_n = 3400 g/mol, f = 2, JenKem Technology USA Inc.) and an MMP-degradable peptide sequence, norbornene-KKGPQG↓IWGQKK-norbornene (M_n = 1595 g/mol, f = 2, Genscript USA) where the ↓ indicates the cleavage site in the peptide. The MMP-degradable peptide used in this work is the same sequence that has been studied previously for other networks designed for cell delivery applications.[32−37] For this work, this sequence is modified with norbornene end groups to form cross-links with PEG-thiol. Since both cross-linkers have norbornene functional groups, network formation takes place through thiol:ene photopolymerization.

All polymer and peptide precursors are used without further modification and are dissolved in 1× phosphate-buffered saline (1× PBS, Gibco) at a concentration of 10 wt %. We make three different networks by varying the amount of PEG-TENB (adaptable cross-linker) and the MMP-cleavable peptide (enzymatically degradable cross-linker). Figure 1 shows a schematic for these networks and the thioester exchange reaction.

Table 1 shows the concentration of each component used for these networks in this work. The first network composition has 1:1 adaptable to MMP-degradable cross-links. In these networks, there is 100% excess thiol, and 50% of the network cross-links are adaptable and 50% are MMP-degradable. A 100% excess thiol means the ratio of the two functional groups, thiol:norbornene, is 2. The network with 3:1 adaptable to MMP-degradable cross-links contains 100% excess thiol with 75% adaptable and 25% enzymatically degradable cross-links. The network with 4:1 adaptable to MMP-degradable cross-links has 60% excess thiol with 80% adaptable cross-links and 20% MMP-degradable cross-links. In these networks, the thiol:norbornene group ratio is 1.6. In this work, we refer to previously characterized fully adaptable networks with 100% excess thiol as a control.[13] We cannot form a fully enzymatically degradable control network with only the MMP-degradable peptide as the cross-linker since these networks do not gel when the thiol:norbornene ratio is 2. MPT measurements for these networks are provided in Figure S1 in the Supporting Information.

The precursor solution contains the polymer and peptide described above and a photocatalyst, lithium phenyl-2,4,6-trimethylbenzoylphosphinate (LAP). This highly water-soluble photocatalyst is synthesized using previously published protocols.[38] To make stock solutions, we dissolve LAP in 1× PBS at 6.8 mM. The final concentration of LAP in the precursor solution is 1 mM. Once LAP is added, the precursor solution is exposed to ultraviolet (UV) light using a light-emitting diode (LED) UV lamp (M365LP1-C1, Thorlabs, Inc.) for 100 s (365 nm, 10 mW/cm^2). A network is formed by a thiol−ene step-growth photopolymerization.[20] For cell encapsulation, 1 mM norbornene-GRGDS (M_n = 611 g/mol, f = 1, Genscript USA) is added to facilitate cellular adhesion.

For MPT measurements of network degradation, 0.15% solids/volume fluorescently labeled functionalized probe particles (Polysciences Inc.) are added to the precursor solutions. Probe particles are functionalized using protocols described in the next section.

https://doi.org/10.1021/acs.macromol.5c00487
Macromolecules 2025, 58, 3872−3885

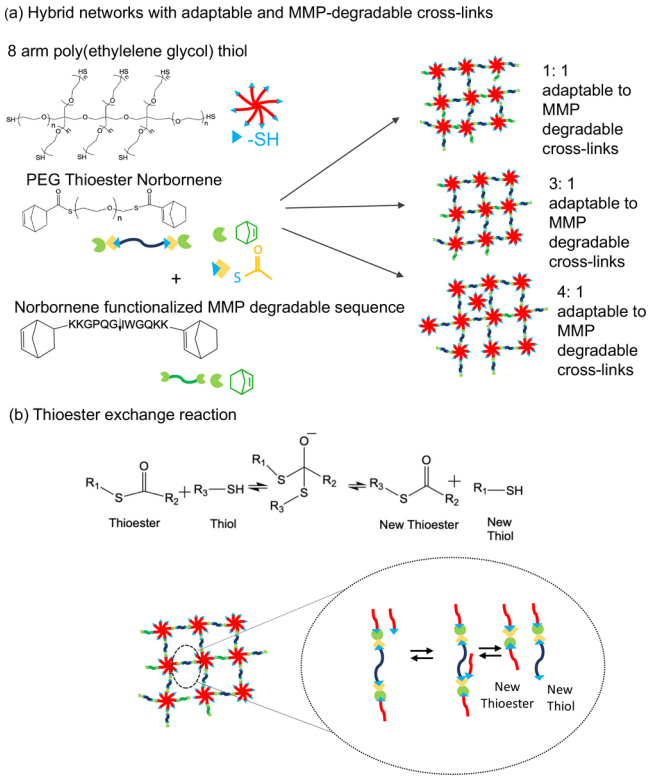

Figure 1. Schematic of designs for hybrid networks and thioester exchange reactions. (a) Hybrid networks in this work are formed by varying the ratio of adaptable to MMP-degradable cross-links. (b) Adaptable cross-links in the presence of excess thiol can undergo an exchange reaction that leads to formation of new thioester and a thiol.

Table 1. Concentrations of Precursors for Each Network

ratio of adaptable to enzymatically degradable cross-links	8-arm PEG-thiol (mM)	PEG-thioester norbornene (mM)	MMP-degradable peptide (mM)	LAP (mM)
1:1	1.1	1.1	1.1	1
3:1	1.1	1.65	0.55	1
4:1	1.1	2.2	0.55	1
control	1.1	2.2	0	1

Probe Particles. For all MPT measurements, surface-modified fluorescently labeled polystyrene particles ($2a$ = 0.97 ± 0.02 μm, where a is the particle radius, Polysciences Inc.) are added at 0.15% solids/volume to the precursor solution. This concentration is dilute enough to limit interparticle interactions but high enough to generate MPT data with good statistics. Probe particles are modified before adding them to the precursor solution using the method described below.

Probe particles used in this work have a short-chain PEG molecule attached to their surface to limit aggregation or interaction with polymers that make up the hydrogel scaffold. These particles will be referred to as PEGylated particles. The surface of the probe is functionalized by covalently tethering methoxy PEG-amine (mPEG-NH_2, M_n = 750 g/mol, Sigma-Aldrich) using the protocol published by Valentine et al.[39] This protocol uses carbodiimide coupling chemistry. In this reaction, the first step is the formation of a reactive *N*-hydroxysuccinimide (NHS) ester and a less stable ester with 1-[3-(dimethylamino)propyl]-3-ethylcarbodiimide (EDC) (Sigma-Aldrich) at pH 6 to activate the carboxylic acid groups on the probe surface. For this step, probe particles are loaded into dialysis tubes (10 kDa molecular weight cutoff, Spectrum Chemicals). These tubes are first submerged in 100 mM 2-N-morpholino ethanesulfonic acid (MES, Sigma-Aldrich) buffer at pH 6 for 2 h. Dialysis tubes containing particles are then rinsed and submerged in MES buffer with 15 mM EDC, 5 mM NHS, and 10-fold excess mPEG-NH_2 for 30 min. After forming activated esters on probe surfaces, probes are then immersed in mPEG-NH_2 at pH 8.5 in borate buffer. This buffer contains 50 mM boric acid (Sigma-Aldrich) and 36 mM sodium tetraborate (Sigma-Aldrich). At pH 8.5, the deprotonation of the amine group on PEG-NH_2 increases. The deprotonated amine group reacts with NHS-ester on the probe surface to form an amine bond. The reaction in borate buffer proceeds for 8 h and is repeated two more times with fresh buffer. After the third reaction, probes are washed with pure borate buffer and stored at 4 °C. These PEGylated probes can be used for several months.[39]

Device Fabrication. To make hydrogels for bulk rheology and MPT measurements, we make sample chambers using glass-bottomed Petri dishes (d = 35 mm, no. 1.5 glass coverslip, MatTek Corporation) and polydimethylsiloxane (PDMS) rings.

PDMS rings are cut from flat sheets of PDMS. PDMS flat sheets are prepared by mixing a silicone elastomer base and curing agent (SYLGARD 184, Dow Corning) at a 10:1 ratio following the manufacturer's protocol. This mixture is degassed in a vacuum oven (Fisher Scientific) and cured at 65 °C overnight.

For bulk rheology, we make PDMS rings with an inner diameter of 8 mm and an outer diameter of 10 mm using biopsy punches (Integra Lifesciences Prod. Corp). PDMS rings are attached to the glass-bottomed Petri dishes using a UV-curable adhesive (NOA-81, Norland Products Inc.) and exposure to UV light. To make gels for bulk rheology experiments, the hydrogel precursor solution is pipetted into the PDMS ring and exposed to UV light to form the gel in the ring. Before bulk rheology measurements, the PDMS ring is removed, and gel samples are taken out of the Petri dishes and placed on the Peltier plate of the rheometer.

For MPT measurements, a PDMS ring with an outer diameter of 8 mm and an inner diameter of 4 mm is cut using biopsy punches (Integra Lifesciences Prod. Corp., Acuderm Inc.) from a flat PDMS sheet. These rings are attached to a glass-bottomed Petri dish using uncured PDMS and cured at 65 °C overnight. Gels are made by adding the precursor solution to the PDMS ring and exposing it to UV light. PDMS rings are used during MPT measurements to limit particle drift during network degradation. To encapsulate hMSCs in networks for cell viability measurements, we use the device made for MPT measurements.

Bulk Rheology. All bulk rheology experiments are performed on an AR-G2 rheometer (TA Instruments). We use an 8 mm sand-blasted parallel plate geometry and all experiments are performed at 37 °C.

All three network compositions in this work are polymerized in the devices described above. To measure the storage modulus of these gels, we remove them from the sample chamber and place them on the rheometer. Before performing a frequency sweep, we determine the strain that is in the linear viscoelastic region. This is done by performing a strain sweep, which is shown in Figure S2 in the Supporting Information for all three networks. Our measurements for all compositions show that the elastic modulus, G', is constant between 0.5 and 2.5% strain at 1 Hz. We then measure the storage modulus in the linear viscoelastic region using frequency sweeps between 0.1 and 1 Hz at 1% strain. We measure 3 replicates for each network composition.

We also measure stress relaxation in all three network compositions. For these experiments, strain is raised to 10% over 10 s and held for 10 min, and the resulting stress is measured. To avoid drying of the hydrogel during the experiment, we use an immersion cup to incubate the gels in 1× PBS during the experiment. Stress relaxation is measured in 3 replicates of each composition.

Network Degradation. We characterize degradation of the three different hydrogel compositions by incubating them in L-cysteine or collagenase and measuring rheological properties using time sweeps. Incubation in L-cysteine degrades the adaptable cross-links in each network using the thioester exchange reaction. Incubation in collagenase enzymatically degrades the MMP-degradable peptide cross-linker. For all degradation experiments, data are measured on a

https://doi.org/10.1021/acs.macromol.5c00487
Macromolecules 2025, 58, 3872−3885

rheometer (AR-G2, TA Instruments) using a time sweep at 1 Hz and 1% strain until the elastic modulus reaches ≈0 Pa or plateaus. In these experiments, hydrogels are incubated in 5 mL of L-cysteine or collagenase solution at 37°C on the rheometer using an immersion cup. We measure degradation of 3 replicates for each composition during each type of degradation.

To characterize network degradation in L-cysteine (Sigma-Aldrich), we incubate networks in 25 mM L-cysteine solution. L-cysteine is an amino acid with a single thiol group. Network degradation occurs due to the exchange reaction between this thiol group and network cross-links. This reaction is similar to the thioester exchange reaction that takes place in the network between excess thiol and network cross-links.[13,40] However, L-cysteine does not become part of the network because it has a single thiol group; therefore, reaction with L-cysteine breaks cross-links. Fully adaptable control hydrogels are incubated in 50 mM L-cysteine solution.[13] This higher concentration of L-cysteine changes the critical transition time, not the microstructure of the network during the phase transition.[26,64] Since the microstructure of the material does not change with the concentration of the degradation buffer, the rheology during hydrogel degradation is comparable between all scaffolds.

To degrade these networks enzymatically, we incubate them in a 0.3 mg/mL collagenase solution (Sigma-Aldrich), which cleaves the MMP-degradable cross-linker. Collagenase is a mixture of enzymes secreted by Clostridium histolyticum.[41−44] The main components are two collagenases, clostripain, and a neutral protease. The activity of our collagenase is 0.25−1 FALGPA units/mg solid and ≤125 CDU/mg solid.[44]

Degradation of all three scaffold compositions in L-cysteine or collagenase is also characterized using multiple particle tracking microrheology (MPT). For bulk rheology and MPT measurements, the same concentration of L-cysteine or collagenase is used. For each network, we measure degradation of three replicates.

Multiple Particle Tracking Microrheology. For MPT measurements, fluorescently labeled PEGylated probe particles are embedded in each sample. We measure Brownian motion of these probe particles using an inverted microscope (Zeiss Observer Z1, Carl Zeiss AG) with a 40× water immersion objective with a low numerical aperture (N.A. 1.2, Carl Zeiss AG). Videos of particle motion are recorded with a high-speed camera (1024 × 1024 pixels, IL5-S SXGA, Fastec Imaging) at a frame rate of 30 frames/s with a 1000 μs exposure time. These parameters balance static and dynamic particle tracking errors in the data.[45,46] Prior to taking MPT measurements, the camera is calibrated using glycerine/water solutions of known concentrations and viscosity. These calibration measurements are shown in Figure S3 in the Supporting Information. MPT measurements of network degradation are performed at 37°C. For network degradation in L-cysteine, we measure 3 replicates of each network.

We use classical particle tracking algorithms to identify the position of each particle in a video using the brightness-weighted centroid. Then we link the position of each particle in each frame using a probability distribution function that accounts for Brownian motion.[46−50] Ensemble-averaged mean-squared displacement of the probe particles (MSD, $\langle \Delta r^2(\tau) \rangle$) is calculated in two dimensions (2D) using

$$\langle \Delta r^2(\tau) \rangle = \langle \Delta x^2(\tau) \rangle + \langle \Delta y^2(\tau) \rangle \quad (1)$$

where τ is the lag time and x and y are position coordinates in 2D. Using the Generalized Stokes−Einstein Relation, rheological properties, such as the creep compliance, can be calculated from the MSDs using

$$\langle \Delta r^2(\tau) \rangle = \frac{k_B T}{\pi a} J(\tau) \quad (2)$$

where a is the radius of the probe particles, $k_B T$ is the thermal energy, and $J(\tau)$ is the creep compliance.

The logarithmic slope of the MSD, defined as

$$\alpha = \frac{d\log\langle \Delta r^2(\tau) \rangle}{d\log \tau} \quad (3)$$

identifies the state of the material. When $\alpha \to 0$, probe particles are arrested in a sample-spanning network and have little to no mobility. When $\alpha = 1$, the material is in the liquid phase and probes freely diffuse through the sample. When α values are between 0 and 1, particle motion is restricted and the material is either a viscoelastic gel or sol.[46,47,49−52] The state of a viscoelastic material is determined by comparing α to the critical relaxation exponent, n, of that material. We use time-cure superposition (TCS) to calculate n.[27,46,47,50,53,54] $\alpha = n$ is the phase transition of the material. When $\alpha < n$, the material is a viscoelastic solid. When $\alpha > n$, the material is a viscoelastic fluid. The procedure for TCS is described in detail in the Results and Discussion.

Cell Culture. Human mesenchymal stem cells (hMSCs) are purchased from RoosterBio in passage 2. To culture cells, we use growth media containing two components, RoosterNourish Basal-MSC-CC and RoosterBooster-GTX, which are used following the manufacturer's protocol. We also add 50 U/mL penicillin/streptomycin (Life Technologies) and 0.5 μg/mL fungizone (Life Technologies) to limit contamination. Cells are cultured in a cell culture Petri dish (150 cm^2 treated cell culture dish, Corning Inc.). They are grown to ≈90% confluency before encapsulating them in hydrogel networks.

Prior to encapsulation, hMSCs are removed from the plate using trypsin-ethylene diamine tetraacetic acid (EDTA) (0.125%, ThermoFisher Scientific). hMSCs are then resuspended in 1× PBS and centrifuged at 2600 RPM for 10 min (Clinical 100, VWR). Cell concentration is measured using a hemacytometer (VWR). hMSCs are added at a final concentration of 2×10^5 cells/mL to the hydrogel precursor solution of each composition. For each composition, we add 17 μL of precursor solution to the MPT sample chamber described above. Gels are polymerized by exposing this precursor solution to UV light.

Once cells are 3D encapsulated in a network, they are incubated in media. This media contains 10% fetal bovine serum (FBS, Life Technologies), 50 U/mL penicillin/streptomycin (Life Technologies), and 0.5 μg/mL fungizone (Life Technologies) in low-glucose Dulbecco's modified Eagle's medium (DMEM, Life Technologies). Gels are kept in an incubator at 37 °C and 5% CO_2. Cell viability is measured 24 h post-encapsulation by performing a live/dead assay.

Live/Dead Assay. We measure viability of encapsulated hMSCs using a live/dead staining assay kit (Invitrogen). Before staining, media is removed from the sample chamber and hydrogels are rinsed with 1× PBS. Live/dead stain is prepared following the manufacturer's protocol. Washed hydrogels are immersed in 200 μL of the staining solution and placed in an incubator at 37 °C for 20 min. After 20 min, hydrogels are removed from the incubator. Before imaging, we wash each hydrogel with 1× PBS to remove excess dye. Images are taken using a Keyence BZ-X 810 fluorescence microscope with a 10× objective. Images are analyzed using ImageJ (U.S. National Institutes of Health) to determine the percentage of viable cells.

RESULTS AND DISCUSSION

The goal of this work is to characterize thioester scaffolds with adaptable and proteolytically degradable cross-links to design materials that mimic physical aspects of the ECM for cell delivery. Using bulk rheology, we characterize the elastic modulus and stress relaxation of these networks. We then measure the degradation of these networks by incubation in L-cysteine or collagenase solution, which degrades the adaptable cross-links or enzymatically degradable cross-links, respectively.

We also characterize the degradation of these scaffolds in L-cysteine using MPT. MPT measurements characterize the evolving microstructure. During degradation, we measure

https://doi.org/10.1021/acs.macromol.5c00487
Macromolecules 2025, 58, 3872−3885

multiple network rearrangements in networks with 1:1 and 4:1 adaptable to MMP-degradable cross-links. We measure fewer network rearrangements in networks with 3:1 adaptable to MMP-degradable cross-links. Data are analyzed using time-cure superposition (TCS), which indicates that networks with 1:1 and 4:1 adaptable to MMP-degradable cross-links have elastic structures at the phase transition and networks with 3:1 adaptable to MMP-degradable cross-links have a structure that ranges from elastic to a more open, porous structure. This supports our degradation measurements, where networks with 3:1 adaptable to MMP-degradable cross-links degrade the fastest because they have the most open network structure. We also measure the viability of encapsulated hMSCs in each network. In all three networks, ≥70% of the cells are alive 24 h after 3D encapsulation. Overall, this work provides new designs of hydrogels that mimic physical aspects of the native ECM and will enable user-specified control over the degradation and mechanical properties of these scaffolds.

Bulk Rheological Characterization. *Storage Modulus Measurements.* We measure the storage modulus, G', of each network composition using frequency sweeps between 0.1 and 5 Hz and 1% strain. Figure 2 shows values of the storage modulus averaged over 0.1−1 Hz and 3 hydrogels for each composition. Networks with 1:1 adaptable to MMP-degradable cross-links have the lowest G' value, $G' = 149 \pm 14$ Pa. Networks with 3:1 adaptable to MMP-degradable cross-links have $G' = 342 \pm 5$ Pa. Networks with 4:1 adaptable to MMP-degradable cross-links have the highest G' value, $G' = 588 \pm 63$ Pa.

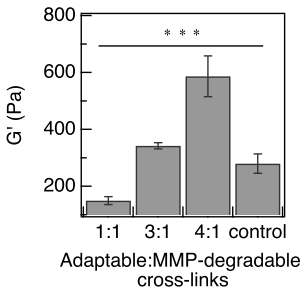

Figure 2. Average storage modulus, G', is plotted for each composition and error bars are the standard deviation from 3 measurements. One-way analysis of variance (ANOVA) followed by Tukey's post hoc test show that there are significant differences in G' between the three network compositions and the control gel, which is a fully adaptable scaffold. *** means $p < 0.001$.

In these materials, the two cross-linkers are of different sizes. The approximate contour length of the MMP-degradable peptide is 4.4 nm, which is estimated from an average contour length of each amino acid of 4 ± 0.2 Å.[55] The estimated contour length of the adaptable cross-linker, PEG-TENB, is ≈30 nm.[56] The adaptable cross-linker is approximately 7× larger than the MMP-degradable cross-linker. The difference in the size of the cross-linkers can lead to the formation of nonidealities in the network, which could reduce the cross-link density.[57−59] For example, PEG-TENB can form loops between arms of the same PEG-thiol molecule. The MMP-degradable cross-linker may not form a cross-link due to the small molecular size, which may cause more dangling ends where only one end of the peptide is tethered to a PEG-thiol. Both of these conformations would reduce cross-link density and lead to decreases in elastic moduli.

We can use this information to interpret the values of G'. Networks with 1:1 adaptable to MMP-degradable cross-links have the lowest value of G', and the MMP-degradable peptide cross-linker is 50% of the network cross-links. We hypothesize that it could be harder for the MMP-degradable cross-linker to make a cross-link and contribute to the network due to the size of the molecules, as described above. In networks with 3:1 adaptable to MMP-degradable cross-links, only 25% of the total cross-links are formed by the MMP-degradable peptide. This results in a higher value of G', since the amount of MMP-degradable cross-links is decreased. Networks with 4:1 adaptable to MMP-degradable cross-links have 60% excess thiol, which makes the total cross-linker concentration the highest. These scaffolds have more thiols available for cross-linking, making the cross-linking reaction more favorable than in the other networks. This results in networks with 4:1 adaptable to MMP-degradable cross-links having higher cross-link density and value of G' than the other two networks.

Our previous work measures $G' = 281 \pm 35$ Pa for fully adaptable networks with 100% excess thiol, which is the control in Figure 2.[13] Networks with 1:1 adaptable to MMP-degradable cross-links have 100% excess thiol, but we measure a lower elastic modulus. This can be due to network defects. In networks with 3:1 adaptable to MMP-degradable cross-links, 25% of the adaptable cross-links from fully adaptable networks are replaced with MMP-degradable cross-links. MMP-degradable cross-links are smaller and can decrease the mesh size of the network, resulting in an increased modulus when compared to the fully adaptable network. In networks with 4:1 adaptable to MMP-degradable cross-links, the MMP-degradable cross-linker is added to the adaptable networks with 100% excess thiol, which decreases the amount of excess thiol to 60%. This increases the cross-link density and results in a higher modulus.

Stress Relaxation Measurements. We measure stress relaxation in all three compositions by applying 10% strain at 1 Hz over 10 s. The resulting stress is measured over 10 min and characterizes material viscoelasticity. Figure 3a shows the average stress relaxation profiles for all three networks and the fully adaptable control gel.[13] The solid lines are the average network response, and the shaded regions are the standard deviation for each composition. In Figure 3a, we measure a decrease in stress for all three compositions. Due to the thioester exchange reaction that takes place in the presence of unreacted network thiol, all compositions can rearrange, leading to a decrease in the initial stress. This stress relaxation response depends on the elastic and viscous components of each network. In these scaffolds, MMP-degradable cross-linkers are the elastic component, and excess thiol and adaptable cross-links are the viscous component that allows the generated stress to decrease. We measure that the stress relaxation profiles of all three network compositions are within the error of each other. This indicates that the stress relaxation properties do not change significantly by the addition of MMP-degradable cross-links or higher cross-link density at physiological pH. Previous work measures that increasing excess thiol can lead to faster stress relaxation in thioester networks that are fully adaptable.[20] In our systems, a decrease in free network thiol or the addition of a nonexchangeable cross-linker such as the MMP-degradable peptide can decrease stress relaxation. Instead, we measure that viscoelasticity is constant regardless of composition and we hypothesize this is because either (1) there are not enough MMP-degradable

https://doi.org/10.1021/acs.macromol.5c00487
Macromolecules 2025, 58, 3872−3885

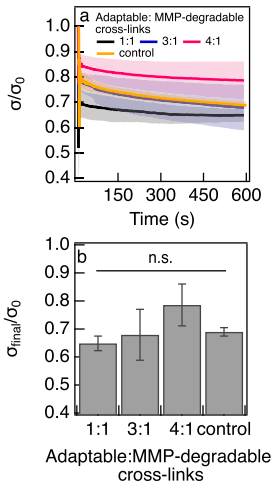

Figure 3. Stress relaxation measurements of the three network compositions and the fully adaptable control gel. Stress relaxation is measured by applying 10% strain to each network for 10 min. (a) Average stress response of each network is the solid line and the standard deviation is the shaded region. The response is measured as the stress, σ, at any time normalized by the initial stress, σ_0. (b) The ratio of the final stress measured at the end of 10 min, σ_{final}, to the initial stress, σ_0, is calculated for each network to measure the extent of stress relaxation in each network. n.s means $p > 0.05$. There is no significant difference in the extent each network relaxes stress.

cross-links in these networks to change the viscoelasticity of the material or (2) network defects from the different sized cross-linkers could be resulting in a constant ratio of viscous and elastic components.

We then calculate the extent of stress relaxation using the ratio of the final stress, σ_{final}, to the initial value of stress, σ_0. These data are shown in Figure 3b. There is no significant difference in the extent of stress relaxation between the three networks. Networks with 1:1 adaptable to MMP-degradable cross-links have the highest concentration of MMP-degradable cross-linker, which should result in the lowest extent of stress relaxation. We hypothesize that network defects can provide a higher amount of free network thiols, which would lead to network rearrangement and a similar extent of stress relaxation as networks with 3:1 and 4:1 adaptable to MMP-degradable cross-links. Networks with 4:1 adaptable to MMP-degradable cross-links have a lower amount of excess thiol, 60% excess thiol. This does not result in a significant decrease in the extent of stress relaxation compared to the other two networks. For fully adaptable control networks, we measure $\sigma_{final}/\sigma_0 = 0.69 \pm 0.02$ in 600 s.[13] These values are similar to those measured in this work. This confirms that the addition of the MMP-degradable cross-linker at varying concentrations to these thioester networks does not alter the viscoelastic nature of the scaffolds.

Network Degradation Using the Thioester Exchange Reaction. We measure network degradation by incubating networks in 25 mM L-cysteine solution. The thiol group from L-cysteine reacts with the thioester cross-links in the network, which causes thioester exchange. This exchange reaction leads to network degradation because L-cysteine has only one functional group, which means it will not be part of the network.

We measure decreases in elastic moduli of all three network compositions as they undergo the thioester exchange reaction with L-cysteine. Figure 4 plots normalized elastic moduli, G'_{norm}, over time for all three compositions. $G'_{norm} = \frac{G'}{G'_0}$, where G'_0 is the initial value of the modulus. We measure the time required for the normalized modulus to reach 0.1, which is different for each network composition. This value quantifies the time required to reduce the initial cross-link density by 90%. The time required to reduce the cross-link density of networks with 1:1 and 3:1 adaptable to MMP-degradable cross-links by 90% is 66 ± 10 and 39 ± 5 min, respectively. Networks with 4:1 adaptable to MMP-degradable cross-links have the longest degradation time, 90 ± 18 min.

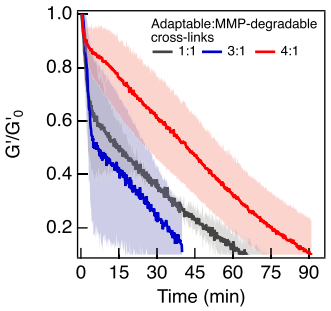

Figure 4. Network degradation for all three compositions is carried out in 0.25 mM L-cysteine. L-Cysteine degrades networks using the thioester exchange reaction. Using time sweep measurements, we measure the change in the elastic modulus, G', over time. We plot normalized elastic moduli, G'_{norm}, which is defined as $G'_{norm} = \frac{G'}{G'_0}$ where G'_0 is the initial elastic modulus value. Data are plotted until $G'_{norm} \approx 0.1$, which is a 90% decrease in moduli and is directly related to the amount of cross-links broken. The solid line is the average value of G'_{norm} from three measurements and the shaded area is the standard deviation.

All three networks have different concentrations of adaptable cross-links that result in different degradation times. Network degradation can also be affected by defects. As discussed in the previous section, there is potential for more defects in networks with 1:1 adaptable to MMP-degradable cross-links, which could slow degradation due to decreased diffusion of L-cysteine through the scaffold and complex architecture during material evolution. Additionally, these networks have the highest number of enzymatically degradable cross-links, which do not degrade in L-cysteine. Networks with 3:1 adaptable to MMP-degradable cross-links have higher concentrations of adaptable cross-links compared to networks with 1:1 adaptable to MMP-degradable cross-links. This means these networks can be degraded easily by thioester exchange, which is measured by faster degradation. Networks with 4:1 adaptable to MMP-degradable cross-links have the highest cross-link density, which is likely the reason these networks are the slowest to degrade. Overall, these data show that even with varying concentrations of adaptable cross-links, these networks can be degraded completely by the thioester exchange reaction initiated by an external source of thiols. This can guide the design of networks for applications where on-demand degradation is required.

Network Degradation in Collagenase. We measure enzymatic degradation of all three network compositions using time sweep measurements. We carry out enzymatic degradation by incubating networks in collagenase. Collagenase contains clostripain and neutral proteases which only break the MMP-degradable cross-linker and do not affect the adaptable cross-links.

https://doi.org/10.1021/acs.macromol.5c00487
Macromolecules 2025, 58, 3872−3885

In Figure 5, we compare the temporal change in G'_{norm} of all three networks. Since each network composition has a different amount of enzymatically degradable cross-links, we measure different extents of degradation. Networks with 1:1 adaptable to MMP-degradable cross-links degrade the fastest, with complete degradation in 42 ± 14 min. These networks have a larger amount of enzymatically degradable cross-links, 50% of the total cross-links. Once a large portion of the MMP-degradable cross-links break, there is no sample-spanning network present since at least 3 cross-links per molecule are required to form a network structure.[57]

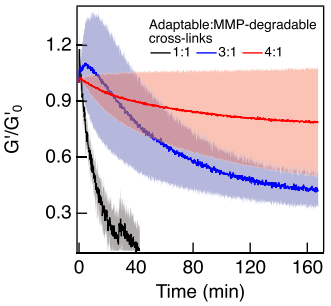

Figure 5. Network degradation for all three compositions is carried out in 0.3 mg/mL collagenase solution. Collagenase degrades MMP-cleavable peptide cross-links. With time sweep measurements, the change in the elastic modulus, G', over time is measured. The plot shows temporal change in normalized elastic moduli, G'_{norm}, which is defined as $G'_{norm} = \frac{G'}{G'_0}$ where G'_0 is the initial elastic modulus value. The solid lines are the average G'_{norm} values and the shaded regions are the standard deviations from three measurements.

Networks with 3:1 adaptable to MMP-degradable cross-links only partially degrade when incubated in collagenase. In these experiments, we measure that the material degrades to 50% of the initial value of G' after ≈2.5 h. In this composition, 25% of the cross-links are enzymatically degradable. After these cross-links degrade, a sample-spanning gel network with thioester cross-links can still be present, which will not degrade in collagenase. After the MMP-degradable cross-links degrade, any further decrease in modulus is likely due to network rearrangement under the applied strain of the bulk rheology measurement.

Networks with 4:1 adaptable to MMP-degradable cross-links are the slowest to degrade and have the lowest extent of degradation after 2.5 h. These networks have the highest cross-link density and only have 20% enzymatically degradable cross-links. G' plateaus at 80% of its initial value, which means that only 20% of the network cross-links are degraded, which are the MMP-degradable cross-links. Also, we measure large deviations in the normalized G' values of networks with 3:1 and 4:1 adaptable to MMP-degradable cross-links. Such large deviations are not measured during the degradation of networks with 1:1 adaptable to MMP-degradable cross-links. These deviations can be the result of shear-induced rearrangement of these partially degraded networks.

These measurements indicate that we can design networks that will only partially degrade by cell-secreted proteases. This can be used in the design of these materials to vary degradability, specifically during cell-mediated degradation, to mimic native niches when these scaffolds are used as cell delivery vehicles.

MPT Measurements during Scaffold Degradation. *Degradation Using L-Cysteine.* We measure the degradation of the three network compositions in a 25 mM solution of L-cysteine using MPT, Figure 6. MPT measures the Brownian motion of fluorescently labeled probe particles embedded in the network and characterizes material properties of the evolving network. In Figure 6, t = 0 min is the time degradation is initiated by incubation in L-cysteine solution. The color of the MSD indicates the time of incubation. Warm colors, such as red, orange, and yellow, indicate short incubation times. Long times are indicated by blue, green, and violet, which are cool colors. In all three networks, the logarithmic slope of the MSD, $\alpha = \frac{d\log\langle\Delta r^2(\tau)\rangle}{d\log\tau}$, and the magnitude of the MSDs increase over time. An increase in α indicates less restricted particle motion and an increase in the magnitude of the MSD measures increased probe diffusivity. When $\alpha < 1$, this is an apparent diffusivity with units of $\mu m^2/s^\alpha$, and when $\alpha = 1$, this is the probe diffusivity. This indicates a decrease in connectivity in the network resulting from the breaking of cross-links. At the end of each experiment, $\alpha \approx 1$ indicates that the material is a sol and probe particles are freely diffusing in all three network compositions.

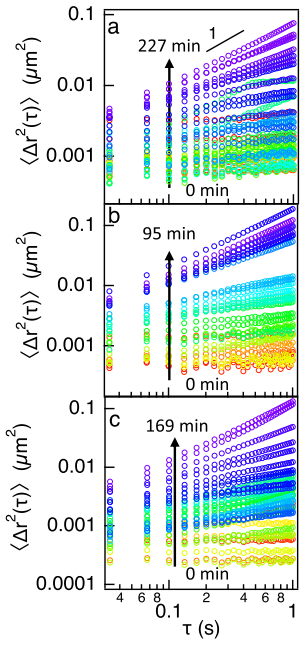

Figure 6. MPT measurements of degradation of all three compositions while they undergo the thioester exchange reaction in response to incubation in L-cysteine. Mean-squared displacements, $\langle\Delta r^2(\tau)\rangle$, measured during degradation of networks with (a) 1:1, (b) 3:1, and (c) 4:1 adaptable to MMP-degradable cross-links. For all three network compositions the magnitude of and the logarithmic slope of the MSD, α, increase over time indicating increased probe mobility and decreased network connectivity.

In Figure 6a, we measure in a scaffold with 1:1 adaptable to MMP-degradable cross-links that the magnitude of the MSDs and α increases over time. This increase is non-monotonic and can be the result of local network rearrangements. After an initial increase in probe mobility, we measure a decrease, indicating that probe particle mobility is becoming more restricted. This phenomenon occurs several times before we measure complete network degradation. We measure the initial

https://doi.org/10.1021/acs.macromol.5c00487
Macromolecules 2025, 58, 3872−3885

value of α changes from $\alpha \approx 0$ to 1 in 227 min, which is the longest measured time to degrade. In networks with 1:1 adaptable to MMP-degradable cross-links, there are 50% MMP-degradable cross-links, which do not undergo the exchange reaction. Also, the MMP-degradable peptide cross-linker has a shorter contour length than the PEG-TENB, which could lead to smaller pore sizes. Smaller pore size can limit the transport of L-cysteine, which can affect the degradation time scale since it takes longer for L-cysteine to completely diffuse into the scaffold.

Figure 6b plots MSDs measured during degradation of networks with 3:1 adaptable to MMP-degradable cross-links. These networks degrade over a shorter period of time, 95 min, compared to the other two networks. These networks have a higher amount of adaptable cross-links compared to networks with 1:1 adaptable to MMP-degradable cross-links, which means there are more cross-links that can undergo thioester exchange with L-cysteine. This results in a shorter degradation time.

MSDs measured during degradation of networks with 4:1 adaptable to MMP-degradable cross-links are shown in Figure 6c. Similar to networks with 1:1 adaptable to MMP-degradable cross-links, we also measure non-monotonic increases in the logarithmic slope and magnitude of the MSDs. We attribute this to network rearrangement resulting in the formation of polymeric clusters and potentially reforming the network structure. The degradation time of this network is 169 min, which is longer than networks with 3:1 adaptable to MMP-degradable cross-links but slower than networks with 1:1 adaptable to MMP-degradable cross-links. Networks with 4:1 adaptable to MMP-degradable cross-links have the highest cross-link density, which increases degradation time, and the most adaptable cross-links, which decreases degradation time, leading to a degradation time between the other two compositions.

Although the sample sizes are different, we measure similar trends in degradation time for MPT and bulk rheology measurements. The time scales measured by MPT are longer compared to bulk rheology measurements. Faster degradation measured with bulk rheology can be due to the addition of externally applied strain in these measurements, which is not present in MPT. Due to the externally applied strain, faster network rearrangement can take place, which could lead to faster degradation.

We also calculate the logarithmic slope of the MSD, α, using eq 3. α measures the change in probe mobility over time and is also indicative of the phase of the material. When $\alpha = 1$, probes are freely diffusing in a liquid, and when $\alpha = 0$, probes are in a sample-spanning network and have little to no mobility. Figure 7a–c shows the change in α values for all three network compositions during degradation. In all three compositions, the initial value of $\alpha \approx 0$ and over time this value increases to 1 as the scaffold degrades. This indicates that there is a phase transition taking place in all of the networks.

Figure 7a shows α values measured during degradation of a network with 1:1 adaptable to MMP-degradable cross-links. The initial α value is ≈0.1, this higher value could be due to initial scaffold swelling. As time progresses, we measure that the α values increase. We also measure a non-monotonic increase in α with time, which we hypothesize is due to network rearrangement during degradation. In our previous work with thioester networks with fully adaptable cross-links, we measured similar non-monotonic increases in α values

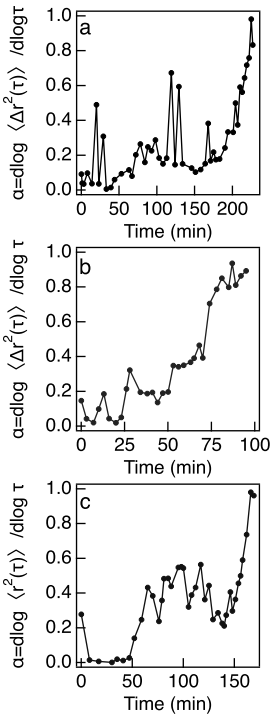

Figure 7. Logarithmic slope of the MSD, $\alpha = \frac{d\log\langle\Delta r^2(\tau)\rangle}{d\log \tau}$, increases as networks degrade by the thioester exchange reaction when incubated in L-cysteine. The value of α is measured with MPT during degradation of networks with (a) 1:1, (b) 3:1, and (c) 4:1 adaptable to MMP-degradable cross-links.

during degradation, which we attribute to network rearrangement.[13] As L-cysteine reacts with adaptable cross-linkers in the networks, more free thiols are generated. These free thiols can exchange with remaining network cross-links, leading to the formation of polymeric clusters or a sample-spanning network. In networks with 1:1 adaptable to MMP-degradable cross-links, degradation is slow, meaning during the majority of the measurement, there is still a network structure which could limit diffusion of untethered thiols out of the network. Due to this, some of the untethered thiols may remain in the network and form new cross-links. Such network rearrangement could result in restricted probe mobility. After undergoing several rearrangements, the value of α reaches 1, which means probes are freely diffusing in a polymeric solution.

Figure 7b shows the change in α values during degradation of a network with 3:1 adaptable to MMP-degradable cross-links. As the exchange reaction with L-cysteine proceeds, network cross-links break and probe mobility increases. This results in an increase in α values. Although the increase in α is non-monotonic, we measure fewer rearrangements compared to networks with 1:1 adaptable to MMP-degradable cross-links. These networks have a higher amount of adaptable cross-links than networks with 1:1 adaptable to MMP-degradable cross-links, meaning the exchange reaction with L-cysteine can lead to rapid loss of structure. Due to this, the untethered polymer can diffuse out of the network quickly and would be unavailable for rearrangement. These networks are the closest in structure to the previously studied fully adaptable networks with 100% excess thiol, which is the control gel in this work.[13] Similar to those networks, we do not always measure network rearrangement in networks with 3:1 adaptable to MMP-

https://doi.org/10.1021/acs.macromol.5c00487
Macromolecules 2025, 58, 3872–3885

degradable cross-links.[13] Additionally, fewer network rearrangements during degradation could also lead to a shorter degradation timescale compared to the other network compositions.

Figure 7c shows changes in α values of a network with 4:1 adaptable to MMP-degradable cross-links. The initial α value is close to 0.3, which can be due to initial swelling in the L-cysteine solution. Similar to other networks, we measure a non-monotonic increase in α values after 60 min. We hypothesize this is the result of network rearrangement that takes place during degradation. In these networks, the high cross-link density can result in a gradual loss of network architecture. This could limit the diffusion of untethered polymers out of the system and lead to the formation of new cross-links that result in network rearrangement similar to networks with 1:1 adaptable to MMP-degradable cross-links.

During degradation, these networks likely undergo a gel−sol transition and may even undergo phase transitions during rearrangement. To pinpoint the gel−sol transition, we analyze our MPT data using time-cure superposition.

Time-Cure Superposition. Using MPT, we measure the phase transition of the three network compositions degraded in L-cysteine solution. A gel is defined as a sample-spanning network structure. We measure a gel−sol phase transition when the last sample-spanning network structure breaks. MPT data are analyzed using time-cure superposition (TCS) to identify this phase transition. TCS is the superposition of viscoelastic functions at different extents of reaction.[27,46,49,50,53,54,60−64] Using TCS, we determine the critical degradation time, t_c, and critical relaxation exponent, n. t_c is the time when the phase transition occurs or the last sample-spanning network cluster breaks.[26,60,63,65] The value of n defines the phase transition and the material structure at the phase transition, as described previously.

To calculate the values of t_c and n, we first sort MSDs based on their distinct curvature at the shortest lag times ($0.03 \leq \tau \leq 1$ s) into either pre- or post-degradation MSDs. Short lag times are chosen because they measure the longest relaxation time of the material. Pre-degradation MSDs or gel MSDs curve downward because the longest relaxation time is of a sample-spanning polymeric network. Post-degradation MSDs or sol MSDs curve upward because they measure the longest relaxation time of a polymer solution.[27,46,49,50,61−64,66] Using shift factor a for the lag time axis and b for the MSD axis, MSD curves are shifted to form sol and gel master curves.

In Figure 8, we provide an example of TCS for a network with 3:1 adaptable to MMP-degradable cross-links. TCS plots for all three hybrid networks are provided in the Supporting Information in Figures S4−S11. MSDs from Figure 5b are shifted to create master curves in Figure 8a. The initial MSDs in the gel master curve in Figure 8a indicate that probes are in a sample-spanning network and have little to no mobility. Moving along the gel master curve, as time increases, probe mobility also increases as the exchange reaction takes place between L-cysteine and network cross-links, and a sample-spanning network structure still exists. As the reaction between L-cysteine and the network continues, the last sample-spanning cluster remains, and the MSD measured is the last curve on the gel master curve. MSDs measured after the last sample-spanning cluster breaks are on the sol master curve, where probe mobility is still restricted due to the presence of polymeric clusters, Figure 8a. Eventually, these polymeric clusters break, and probe motion becomes freely diffusive in a

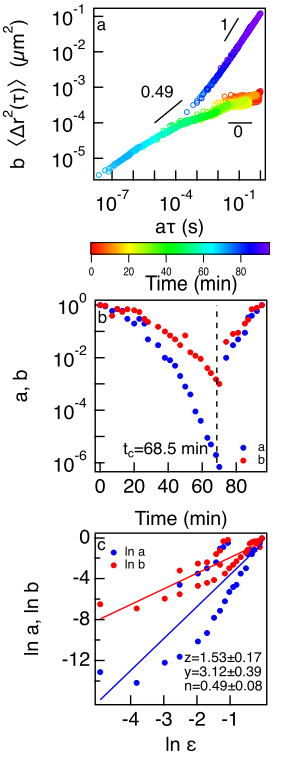

Figure 8. Time-cure superposition of a network with 3:1 adaptable to MMP-degradable cross-links. (a) MSDs from Figure 5b are shifted into sol and gel master curves using shift factors a and b. (b) Shift factors a and b go to zero at the critical degradation time, t_c = 68.5 min. (c) y and z are calculated by plotting the logarithm of shift factors a and b against the logarithm of the distance away from the critical degradation time, $\epsilon = \frac{|t - t_c|}{t_c}$. The critical relaxation exponent, n, is calculated from the ratio of scaling exponents y and z.

polymer solution. Where these two master curves meet is the phase transition, and the slope at this point is the critical relaxation exponent, n.

The value of n is calculated from shift factors a and b, which are used to create the two master curves.[26,53,63,65] Shift factor a is related to the longest relaxation time, τ_L, and the distance away from the critical extent of degradation, $\epsilon = \frac{|t - t_c|}{t_c}$, by scaling exponent y using

$$a \sim \tau_L^{-1} \sim \left(\frac{|t - t_c|}{t_c}\right)^y \tag{4}$$

Shift factor b is related to the inverse of the steady-state creep compliance, J_e^{-1}, and ϵ by scaling exponent z by[53,60,63,65]

$$b \sim J_e^{-1} \sim \left(\frac{|t - t_c|}{t_c}\right)^z \tag{5}$$

The ratio of these two exponents is the value of n

$$n = \frac{z}{y} \tag{6}$$

Shift factors a and b are plotted against time in Figure 8b to calculate the critical degradation time, t_c. t_c is when the last sample-spanning cluster breaks. The values of shift factors a and b approach 0 at t_c. This is a measure of the elastic modulus of the network approaching zero in the gel and the viscosity

https://doi.org/10.1021/acs.macromol.5c00487
Macromolecules 2025, 58, 3872−3885

becoming infinite in the sol.[60,66] Both τ_L and J_e have power law behavior before and after the gel point.[46,53,66] In Figure 8c, the logarithm of the shift factors is plotted versus the logarithm of the distance away from critical degradation time, ln ϵ. Based on gelation theory, they are fit to a line.[67] While the linear fit does not capture network rearrangement, this method still gives an accurate measure of the critical relaxation exponent, n, of the network. The values of the critical scaling exponents y and z are calculated from this fit, which is described by eqs 4 and 5. Once these values are known, the value of n is calculated using eq 6. We compare the critical relaxation exponent and critical degradation time for all three network compositions.

The values of the average critical relaxation exponent, n_{avg}, and average critical degradation time, $t_{c,avg}$, for all three networks are provided in Table 2. The value of n defines the phase transition and is also indicative of the network structure at the phase transition. When $0 < n < 0.5$, the material is a densely cross-linked elastic network that stores energy. When $0.5 < n < 1$, the network has an open structure and dissipates more energy than it stores.[26,53,68] We calculate errors for each n value by propagating errors in y and z, which are propagated when the average value of n is calculated.

Table 2. Critical Values Measured during Network Degradation

ratio of adaptable to MMP-degradable cross-links	average critical relaxation exponent, n_{avg}	average critical degradation time, $t_{c,avg}$ (min)
1:1	0.30 ± 0.07	111.4 ± 18
3:1	0.45 ± 0.09	65.1 ± 15
4:1	0.34 ± 0.08	139.0 ± 17
control	0.53 ± 0.12	15.1 ± 7.8

Our measurements indicate that all three network compositions have $n_{avg} < 0.5$. This means all compositions form elastic networks that store more energy than they dissipate. Also, these networks have n values that are within error of each other, indicating the network microstructure is similar regardless of the composition. The n_{avg} values of networks with 1:1 and 4:1 adaptable to MMP-degradable cross-links suggest they only form tightly cross-linked networks. The n_{avg} value of networks with 3:1 adaptable to MMP-degradable cross-links indicates that this composition forms networks that range from elastic to more open networks.

The structure of the networks in this study is similar to previously characterized thioester networks that only have adaptable cross-links. Networks with 1:1 and 4:1 adaptable to MMP-degradable cross-links have n_{avg} values similar to fully adaptable networks with 0% excess thiol, where $n_{avg} = 0.34 \pm 0.07$. These networks are elastic in nature because there are fewer excess thiols available for rearrangement.[13] In this work, even though there are excess thiols present in networks with 1:1 adaptable to MMP-degradable cross-links, the addition of MMP-degradable cross-links makes their structure more elastic. In networks with 4:1 adaptable to MMP-degradable cross-links, the reduced excess thiol and presence of the MMP-degradable cross-linker make the network structure more elastic.

Networks with 3:1 adaptable to MMP-degradable cross-links have structures that range from elastic to open networks. These networks are slightly more elastic compared to fully adaptable networks with 100% excess thiol that were characterized previously.[13] Fully adaptable control networks have a structure that can range from elastic to a more open, porous network with $n_{avg} = 0.53 \pm 0.12$.[13] The more elastic nature of the hybrid network is likely due to the addition of the MMP-degradable peptide, which does not take part in rearrangement. Networks with 3:1 adaptable to MMP-degradable cross-links also have the most open structure, which explains why these materials consistently degrade the fastest.

Once we measure n values for each network composition, we plot α values with the phase transition region in Figure S12 in the Supporting Information. We measure network rearrangement results in the formation of a sample-spanning network for networks with 1:1 and 4:1 adaptable to MMP-degradable cross-links. As discussed in the previous section, in networks with 1:1 and 4:1 adaptable to MMP-degradable cross-links, the presence of MMP-degradable cross-links can cause more gradual degradation. Due to this, untethered network thiols may not easily diffuse out of the network, which could lead to network reformation. Networks with 3:1 adaptable to MMP-degradable cross-links undergo fewer network rearrangements, which do not lead to reformation of a sample-spanning network. In these networks, most of the network cross-links are adaptable, and the material has a looser network structure. Once the adaptable cross-links undergo the exchange reaction, there is a rapid loss of structure, leading to fewer network arrangements.

We also compare the average critical degradation time, $t_{c,avg}$, for each network. $t_{c,avg}$ values for networks with 1:1 and 4:1 adaptable to MMP-degradable cross-links are within error of each other. In both these networks, we measure multiple network rearrangements that reform sample-spanning networks during degradation. These rearrangements likely slow overall degradation. Networks with 3:1 adaptable to MMP-degradable cross-links are the fastest to degrade, which we hypothesize is correlated with fewer network rearrangements during degradation and a looser network structure. The trend measured for $t_{c,avg}$ is similar to the trend measured in network degradation time with bulk rheology. The data for fully adaptable control networks are measured with a higher L-cysteine concentration of 50 mM, which leads to the shortest $t_{c,avg}$.[13]

These results indicate that network degradation time and microstructure can be tuned by changing the amount of excess thiol and enzymatically degradable cross-links in the network. Decreasing excess thiol or adding enzymatically degradable cross-links increases the elastic component of the network and increases degradation time.

MPT Measurements of Enzymatic Degradation. We incubate all network compositions in 0.3 mg/mL collagenase to measure enzymatic degradation. Figure S13 in the Supporting Information shows data measured for all networks immediately and 2 days after incubation in collagenase. These networks do not degrade in collagenase over this time period. Although we measure complete degradation of 1:1 adaptable to MMP-degradable cross-links using bulk rheology, we do not measure any degradation with MPT 48 h after incubation. This could indicate that the shear applied during bulk rheological characterization is causing network degradation. In networks with 3:1 and 4:1 adaptable to MMP-degradable cross-links, the MMP-degradable peptide contributes 25 and 20% of the total cross-links. These networks may not degrade completely in collagenase because the majority of the network cross-links are formed by PEG-TENB, which would not be degraded by collagenase.

https://doi.org/10.1021/acs.macromol.5c00487
Macromolecules 2025, 58, 3872−3885

Cell Viability. We 3D encapsulate hMSCs in a network and measure viability after 24 h in all three network compositions. Viability is measured in 4 gels for each network, and in each gel, we take images in 3 different regions, Figure 9. The

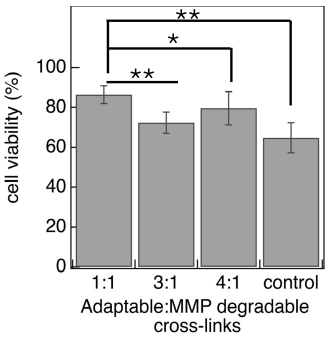

Figure 9. Average viability of hMSCs 24 h after 3D encapsulation in the three hybrid networks and fully adaptable control networks.[69] Viability measurements are presented as the average of measurements in four hydrogels and the error bars are the standard deviation. * and ** represent $p < 0.05$ and $p < 0.01$, respectively.

number of live cells is reported as the average of all measurements. Representative images of live/dead cell data are shown in Figure S14 in the Supporting Information. In all three networks, we measure that more than 70% of cells are viable. Networks with 1:1 adaptable to MMP-degradable cross-links have a significantly higher percentage of viable cells compared to the other two networks, 87 ± 4% viable cells. Higher viability in these networks can be the result of a low cross-link density and a higher amount of MMP-degradable cross-links. In networks with 3:1 and 4:1 adaptable to MMP-degradable cross-links, we measure 72 ± 5 and 80 ± 8% viable cells, respectively. In fully adaptable control networks, we measure much lower viability, 64 ± 8%.[69] Viability measured in fully adaptable control networks is similar to viability measured in other adaptable networks with different chemistry but similar viscoelastic properties.[70] The reduced cell viability in networks with 3:1 and 4:1 adaptable to MMP-degradable cross-links compared to networks with 1:1 adaptable to MMP-degradable cross-links is likely due to the increased amount of adaptable cross-links, which tends to lower cell viability.

CONCLUSIONS

In this work, we design and characterize hybrid networks with adaptable thioester and enzymatically degradable peptide cross-linkers. The two cross-linkers have different contour lengths, which we measure leads to non-monotonic changes in rheological properties likely due to network nonidealities. We measure the elastic modulus, G', of networks with varying ratios of adaptable to MMP-degradable cross-links using bulk rheology. As the adaptable MMP-degradable cross-link ratio increases, an increased value of G' is measured. Higher values of G' are a measure of higher cross-link density, which indicates that as the ratio of cross-linkers changes to a higher concentration of adaptable cross-links, network formation is the preferred reaction. This means there is a decrease in nonidealities likely due to a higher concentration of a single cross-linker resulting in a more uniform network structure. The extent of stress relaxation in these networks does not vary significantly with composition. These results show we can tune the moduli of these networks without changing the viscoelastic properties, which is desirable when mimicking the complex properties of tissues. To determine the role of each of the cross-linkers, we degrade them separately. We measure the degradation of these networks in L-cysteine and collagenase using bulk rheology and MPT. These networks rearrange during L-cysteine degradation and have structures at the phase transition that range from elastic (1:1 and 4:1 adaptable to MMP-degradable cross-links) to open network structures (3:1 adaptable to MMP-degradable cross-links). This indicates that the adaptable cross-links are the dominant cross-linker in network formation and are the major factor that sets the properties of the material. These results show that the microstructure of these hybrid materials can be tuned by varying the composition, while properties of each type of cross-linker are maintained to varying degrees. Finally, cell viability measurements show that increasing MMP-degradable cross-links increases the number of viable cells in these thioester scaffolds. Adaptable cross-links enable facile rearrangement, but to maintain cell viability, the cells need an elastic network for attachment, spreading, and, ultimately, motility. This shows that a balance in material viscoelasticity is needed to enable high cell viability and basic cellular processes.

The hybrid networks in this work could better mimic aspects of the native ECM, balancing the viscous and elastic components of the scaffold, which can be done by varying the concentration of adaptable and enzymatically degradable cross-links. There is a trade-off to using these cross-linkers that needs to be considered when designing these materials for their specific application. The enzymatically degradable cross-links play a smaller role in network formation but provide vital elasticity, which enables cell viability and motility. The adaptable cross-linker is the main contributor to network formation and provides dynamic rheological properties, but does not provide the needed elasticity for high cell viability. To use these microenvironments to instruct cell processes, these results must be considered, and a balance must be struck to create materials that enhance cell delivery and promote tissue regeneration. Cell-material interactions in these networks and their ability to deliver cells will be explored in future work.

ASSOCIATED CONTENT

Supporting Information

The following files are available free of charge. The Supporting Information is available free of charge at https://pubs.acs.org/doi/10.1021/acs.macromol.5c00487.

Networks with fully enzymatically degradable cross-links: MSDs measured of 3 replicates containing 8-arm PEG-thiol and MMP-degradable peptide cross-linker with thiol:norbornene ratio of 2 and photocatalyst LAP after UV exposure of 100 *s*; bulk rheological characterization: strain sweeps of all three network compositions measured at 0.1−5% strain and 1 Hz frequency; MPT calibration: mean-squared displacements (MSDs) of 1 μm probes are measured in different concentrations of glycerine solutions; time-cure superposition: time-cure superposition of networks with 1:1 adaptable to MMP-degradable cross-links (replicate 1); time-cure superposition: time-cure superposition of networks with 1:1 adaptable to MMP-degradable cross-links (replicate 2); time-cure superposition: time-cure superposition of networks with 1:1 adaptable to MMP-degradable cross-links (replicate 3); time-cure superposition: time-

https://doi.org/10.1021/acs.macromol.5c00487
Macromolecules 2025, 58, 3872−3885

cure superposition of networks with 3:1 adaptable to MMP-degradable cross-links (replicate 2); time-cure superposition: time-cure superposition of networks with 3:1 adaptable to MMP-degradable cross-links (replicate 3); time-cure superposition: time-cure superposition of networks with 4:1 adaptable to MMP-degradable cross-links (replicate 1); time-cure superposition: time-cure superposition of networks with 4:1 adaptable to MMP-degradable cross-links (replicate 2); time-cure superposition: time-cure superposition of networks with 4:1 adaptable to MMP-degradable cross-links (replicate 3); network rearrangement during scaffold degradation: α values measured during the degradation of all three networks plotted with the transition region; MPT measurements of networks in collagenase: MPT measurements of thioester networks with 3:1 and 4:1 adaptable to MMP-degradable cross-links incubated in collagenase; and cell viability: representative images of viability of hMSCs 24 h after 3D encapsulation in the three network compositions (PDF)

AUTHOR INFORMATION

Corresponding Author

Kelly M. Schultz − *Davidson School of Chemical Engineering, Purdue University, West Lafayette, Indiana 47907, United States;* orcid.org/0000-0001-9040-126X; Email: kmschultz@purdue.edu

Authors

Shivani Desai − *Department of Chemical and Biomolecular Engineering, Lehigh University, Bethlehem, Pennsylvania 18015, United States*

Gautam V. Khare − *Davidson School of Chemical Engineering, Purdue University, West Lafayette, Indiana 47907, United States*

Kristi S. Anseth − *Department of Chemical and Biological Engineering, University of Colorado at Boulder, Boulder, Colorado 80309, United States;* orcid.org/0000-0002-5725-5691

Complete contact information is available at: https://pubs.acs.org/10.1021/acs.macromol.5c00487

Notes

The authors declare no competing financial interest.

ACKNOWLEDGMENTS

Research reported in this publication was supported in part by the National Institute of General Medical Sciences of the National Institutes of Health under award numbers R15GM119065 and R35GM147043. The content is solely the responsibility of the authors and does not necessarily represent the official views of the National Institutes of Health.

REFERENCES

(1) Ehrbar, M.; Sala, A.; Lienemann, P.; Ranga, A.; Mosiewicz, K.; Bittermann, A.; Rizzi, S.; Weber, F. E.; Lutolf, M. Elucidating the role of matrix stiffness in 3D cell migration and remodeling. *Biophysical journal* **2011**, *100*, 284−293.

(2) Stowers, R. S.; Shcherbina, A.; Israeli, J.; Gruber, J. J.; Chang, J.; Nam, S.; Rabiee, A.; Teruel, M. N.; Snyder, M. P.; Kundaje, A.; Chaudhuri, O. Matrix stiffness induces a tumorigenic phenotype in mammary epithelium through changes in chromatin accessibility. *Nat. Biomed. Eng.* **2019**, *3*, 1009−1019.

(3) Engler, A. J.; Sen, S.; Sweeney, H. L.; Discher, D. E. Matrix elasticity directs stem cell lineage specification. *Cell* **2006**, *126*, 677−689.

(4) Elosegui-Artola, A.; Gupta, A.; Najibi, A. J.; Seo, B. R.; Garry, R.; Tringides, C. M.; de Lázaro, I.; Darnell, M.; Gu, W.; Zhou, Q.; Weitz, D. A.; Mahadevan, L.; Mooney, D. J. Matrix viscoelasticity controls spatiotemporal tissue organization. *Nat. Mater.* **2023**, *22*, 117−127.

(5) Khetan, S.; Guvendiren, M.; Legant, W. R.; Cohen, D. M.; Chen, C. S.; Burdick, J. A. Degradation-mediated cellular traction directs stem cell fate in covalently crosslinked three-dimensional hydrogels. *Nature materials* **2013**, *12*, 458−465.

(6) Feng, Q.; Zhu, M.; Wei, K.; Bian, L. Cell-mediated degradation regulates human mesenchymal stem cell chondrogenesis and hypertrophy in MMP-sensitive hyaluronic acid hydrogels. *PLoS One* **2014**, *9*, No. e99587.

(7) Madl, C. M.; LeSavage, B. L.; Dewi, R. E.; Lampe, K. J.; Heilshorn, S. C. Matrix remodeling enhances the differentiation capacity of neural progenitor cells in 3D hydrogels. *Adv. Sci.* **2019**, *6*, No. 1801716.

(8) Kloxin, C. J.; Scott, T. F.; Adzima, B. J.; Bowman, C. N. Covalent adaptable networks (CANs): a unique paradigm in cross-linked polymers. *Macromolecules* **2010**, *43*, 2643−2653.

(9) Kloxin, C. J.; Bowman, C. N. Covalent adaptable networks: smart, reconfigurable and responsive network systems. *Chem. Soc. Rev.* **2013**, *42*, 7161−7173.

(10) Wang, H.; Heilshorn, S. C. Adaptable hydrogel networks with reversible linkages for tissue engineering. *Adv. Mater.* **2015**, *27*, 3717−3736.

(11) Tang, S.; Richardson, B. M.; Anseth, K. S. Dynamic covalent hydrogels as biomaterials to mimic the viscoelasticity of soft tissues. *Prog. Mater. Sci.* **2021**, *120*, No. 100738.

(12) Purcell, B. P.; Lobb, D.; Charati, M. B.; Dorsey, S. M.; Wade, R. J.; Zellars, K. N.; Doviak, H.; Pettaway, S.; Logdon, C. B.; Shuman, J. A.; et al. Injectable and bioresponsive hydrogels for on-demand matrix metalloproteinase inhibition. *Nat. Mater.* **2014**, *13*, 653−661.

(13) Desai, S.; Carberry, B. J.; Anseth, K. S.; Schultz, K. M. Characterizing rheological properties and microstructure of thioester networks during degradation. *Soft Matter* **2023**, *19*, 7429−7442.

(14) McKinnon, D. D.; Domaille, D. W.; Cha, J. N.; Anseth, K. S. Bis-aliphatic hydrazone-linked hydrogels form most rapidly at physiological pH: identifying the origin of hydrogel properties with small molecule kinetic studies. *Chem. Mater.* **2014**, *26*, 2382−2387.

(15) McKinnon, D.; Domaille, D.; Brown, T.; Kyburz, K.; Kiyotake, E.; Cha, J.; Anseth, K. Measuring cellular forces using bis-aliphatic hydrazone crosslinked stress-relaxing hydrogels. *Soft Matter* **2014**, *10*, 9230−9236.

(16) Richardson, B. M.; Wilcox, D. G.; Randolph, M. A.; Anseth, K. S. Hydrazone covalent adaptable networks modulate extracellular matrix deposition for cartilage tissue engineering. *Acta biomaterialia* **2019**, *83*, 71−82.

(17) Tang, S.; Ma, H.; Tu, H.-C.; Wang, H.-R.; Lin, P.-C.; Anseth, K. S. Adaptable Fast Relaxing Boronate-Based Hydrogels for Probing Cell−Matrix Interactions. *Adv. Sci.* **2018**, *5*, No. 1800638.

(18) Hong, S. H.; Kim, S.; Park, J. P.; Shin, M.; Kim, K.; Ryu, J. H.; Lee, H. Dynamic bonds between boronic acid and alginate: hydrogels with stretchable, self-healing, stimuli-responsive, remoldable, and adhesive properties. *Biomacromolecules* **2018**, *19*, 2053−2061.

(19) Smithmyer, M. E.; Deng, C. C.; Cassel, S. E.; LeValley, P. J.; Sumerlin, B. S.; Kloxin, A. M. Self-healing boronic acid-based hydrogels for 3D co-cultures. *ACS macro letters* **2018**, *7*, 1105−1110.

(20) Brown, T. E.; Carberry, B. J.; Worrell, B. T.; Dudaryeva, O. Y.; McBride, M. K.; Bowman, C. N.; Anseth, K. S. Photopolymerized dynamic hydrogels with tunable viscoelastic properties through thioester exchange. *Biomaterials* **2018**, *178*, 496−503.

(21) Carberry, B. J.; Rao, V. V.; Anseth, K. S. Phototunable viscoelasticity in hydrogels through thioester exchange. *Annals of biomedical engineering* **2020**, *48*, 2053−2063.

(22) Koehler, K. C.; Alge, D. L.; Anseth, K. S.; Bowman, C. N. A Diels−Alder modulated approach to control and sustain the release of

dexamethasone and induce osteogenic differentiation of human mesenchymal stem cells. *Biomaterials* **2013**, *34*, 4150−4158.
(23) Metkari, A. S.; Fowler, E. W.; Witt, R. L.; Jia, X. Matrix Degradability Contributes to the Development of Salivary Gland Progenitor Cells with Secretory Functions. *ACS Appl. Mater. Interfaces* **2023**, *15*, 32148−32161.
(24) Tseng, Y.; An, K. M.; Wirtz, D. Microheterogeneity controls the rate of gelation of actin filament networks. *J. Biol. Chem.* **2002**, *277*, 18143−18150.
(25) Sato, J.; Breedveld, V. Transient rheology of solvent-responsive complex fluids by integrating microrheology and microfluidics. *J. Rheol.* **2006**, *50*, 1−19.
(26) Schultz, K. M.; Baldwin, A. D.; Kiick, K. L.; Furst, E. M. Gelation of covalently cross-linked PEG-heparin hydrogels. *Macromolecules* **2009**, *42*, 5310−5316.
(27) Wehrman, M. D.; Lindberg, S.; Schultz, K. M. Quantifying the dynamic transition of hydrogenated castor oil gels measured via multiple particle tracking microrheology. *Soft Matter* **2016**, *12*, 6463−6472.
(28) Meleties, M.; Britton, D.; Katyal, P.; Lin, B.; Martineau, R. L.; Gupta, M. K.; Montclare, J. K. High-Throughput Microrheology for the Assessment of Protein Gelation Kinetics. *Macromolecules* **2022**, *55*, 1239−1247.
(29) Zhang, H.; Wehrman, M. D.; Schultz, K. M. Structural changes in polymeric gel scaffolds around the overlap concentration. *Front. Chem.* **2019**, *7*, 317.
(30) Meleties, M.; Martineau, R. L.; Gupta, M. K.; Montclare, J. K. Particle-Based Microrheology As a Tool for Characterizing Protein-Based Materials. *ACS Biomaterials Science & Engineering* **2022**, *8*, 2747−2763.
(31) Hafner, J.; Oelschlaeger, C.; Willenbacher, N. Microrheology imaging of fiber suspensions−a case study for lyophilized collagen I in HCl solutions. *Soft Matter* **2020**, *16*, 9014−9027.
(32) Anderson, S. B.; Lin, C.-C.; Kuntzler, D. V.; Anseth, K. S. The performance of human mesenchymal stem cells encapsulated in cell-degradable polymer-peptide hydrogels. *Biomaterials* **2011**, *32*, 3564−3574.
(33) Kyburz, K. A.; Anseth, K. S. Three-dimensional hMSC motility within peptide-functionalized PEG-based hydrogels of varying adhesivity and crosslinking density. *Acta biomaterialia* **2013**, *9*, 6381−6392.
(34) Ki, C. S.; Shih, H.; Lin, C.-C. Effect of 3D matrix compositions on the efficacy of EGFR inhibition in pancreatic ductal adenocarcinoma cells. *Biomacromolecules* **2013**, *14*, 3017−3026.
(35) Hao, Y.; Shih, H.; Muňoz, Z.; Kemp, A.; Lin, C.-C. Visible light cured thiol-vinyl hydrogels with tunable degradation for 3D cell culture. *Acta biomaterialia* **2014**, *10*, 104−114.
(36) Sridhar, B. V.; Brock, J. L.; Silver, J. S.; Leight, J. L.; Randolph, M. A.; Anseth, K. S. Development of a cellularly degradable PEG hydrogel to promote articular cartilage extracellular matrix deposition. *Adv. Healthcare Mater.* **2015**, *4*, 702−713.
(37) Arkenberg, M. R.; Dimmitt, N. H.; Johnson, H. C.; Koehler, K. R.; Lin, C.-C. Dynamic click hydrogels for xeno-free culture of induced pluripotent stem cells. *Adv. Biosyst.* **2020**, *4*, No. 2000129.
(38) Fairbanks, B. D.; Schwartz, M. P.; Halevi, A. E.; Nuttelman, C. R.; Bowman, C. N.; Anseth, K. S. A versatile synthetic extracellular matrix mimic via thiol-norbornene photopolymerization. *Advanced materials* **2009**, *21*, 5005−5010.
(39) Valentine, M.; Perlman, Z.; Gardel, M.; Shin, J. H.; Matsudaira, P.; Mitchison, T.; Weitz, D. Colloid surface chemistry critically affects multiple particle tracking measurements of biomaterials. *Biophysical journal* **2004**, *86*, 4004−4014.
(40) Carberry, B. J.; Hernandez, J. J.; Dobson, A.; Bowman, C. N.; Anseth, K. S. Kinetic Analysis of Degradation in Thioester Cross-linked Hydrogels as a Function of Thiol Concentration, p K a, and Presentation. *Macromolecules* **2022**, *55*, 2123−2129.
(41) Mallya, S. K.; Mookhtiar, K. A.; Van Wart, H. E. Kinetics of hydrolysis of type I, II, and III collagens by the class I and II Clostridium histolyticum collagenases. *Journal of protein chemistry* **1992**, *11*, 99−107.
(42) Schultz, K. M.; Baldwin, A. D.; Kiick, K. L.; Furst, E. M. Measuring the modulus and reverse percolation transition of a degrading hydrogel. *ACS macro letters* **2012**, *1*, 706−708.
(43) Wassenaar, J. W.; Braden, R. L.; Osborn, K. G.; Christman, K. L. Modulating in vivo degradation rate of injectable extracellular matrix hydrogels. *J. Mater. Chem. B* **2016**, *4*, 2794−2802.
(44) Mazzeo, M. S.; Chai, T.; Daviran, M.; Schultz, K. M. Characterization of the kinetics and mechanism of degradation of human mesenchymal stem cell-laden poly (ethylene glycol) hydrogels. *ACS applied bio materials* **2019**, *2*, 81−92.
(45) Savin, T.; Doyle, P. S. Static and dynamic errors in particle tracking microrheology. *Biophysical journal* **2005**, *88*, 623−638.
(46) Furst, E. M.; Squires, T. M. *Microrheology*; Oxford University Press, 2017.
(47) Mason, T. G. Estimating the viscoelastic moduli of complex fluids using the generalized Stokes−Einstein equation. *Rheologica acta* **2000**, *39*, 371−378.
(48) Crocker, J. C.; Grier, D. G. Methods of digital video microscopy for colloidal studies. *J. Colloid Interface Sci.* **1996**, *179*, 298−310.
(49) Larsen, T. H. Microrheology of responsive hydrogels. Ph.D. thesis, University of Delaware, 2008.
(50) Schultz, K. M.; Furst, E. M. Microrheology of biomaterial hydrogelators. *Soft Matter* **2012**, *8*, 6198−6205.
(51) Waigh, T. A. Microrheology of complex fluids. *Rep. Prog. Phys.* **2005**, *68*, 685.
(52) Mason, T. G.; Ganesan, K.; van Zanten, J. H.; Wirtz, D.; Kuo, S. C. Particle tracking microrheology of complex fluids. *Physical review letters* **1997**, *79*, 3282.
(53) Adolf, D.; Martin, J. E. Time-cure superposition during crosslinking. *Macromolecules* **1990**, *23*, 3700−3704.
(54) McGlynn, J. A.; Wu, N.; Schultz, K. M. Multiple particle tracking microrheological characterization: Fundamentals, emerging techniques and applications. *J. Appl. Phys.* **2020**, *127*, 201101.
(55) Ainavarapu, S. R. K.; Brujić, J.; Huang, H. H.; Wiita, A. P.; Lu, H.; Li, L.; Walther, K. A.; Carrion-Vazquez, M.; Li, H.; Fernandez, J. M. Contour length and refolding rate of a small protein controlled by engineered disulfide bonds. *Biophysical journal* **2007**, *92*, 225−233.
(56) Kienberger, F.; Pastushenko, V. P.; Kada, G.; Gruber, H. J.; Riener, C.; Schindler, H.; Hinterdorfer, P. Static and dynamical properties of single poly (ethylene glycol) molecules investigated by force spectroscopy. *Single Molecules* **2000**, *1*, 123−128.
(57) Rubinstein, M.; Colby, R. H. *Polymer physics*; Oxford University Press: New York, 2003; vol *23*.
(58) Lutolf, M.; Hubbell, J. Synthesis and physicochemical characterization of end-linked poly (ethylene glycol)-co-peptide hydrogels formed by Michael-type addition. *Biomacromolecules* **2003**, *4*, 713−722.
(59) Saffer, E. M.; Lackey, M. A.; Griffin, D. M.; Kishore, S.; Tew, G. N.; Bhatia, S. R. SANS study of highly resilient poly (ethylene glycol) hydrogels. *Soft Matter* **2014**, *10*, 1905−1916.
(60) Winter, H. H.; Winter, H. Evolution of rheology during chemical gelation. In *Permanent and Transient Networks*; Steinkopff, 1987; pp 104−110.
(61) Wu, N.; Schultz, K. M. Microrheological characterization of covalent adaptable hydrogels for applications in oral delivery. *Soft Matter* **2019**, *15*, 5921−5932.
(62) Winter, H. H. Can the gel point of a cross-linking polymer be detected by the G−G crossover? *Polym. Eng. Sci.* **1987**, *27*, 1698−1702.
(63) Chambon, F.; Winter, H. H. Linear viscoelasticity at the gel point of a crosslinking PDMS with imbalanced stoichiometry. *J. Rheol.* **1987**, *31*, 683−697.
(64) Schultz, K. M.; Anseth, K. S. Monitoring degradation of matrix metalloproteinases-cleavable PEG hydrogels via multiple particle tracking microrheology. *Soft Matter* **2013**, *9*, 1570−1579.

https://doi.org/10.1021/acs.macromol.5c00487
Macromolecules 2025, 58, 3872−3885

(65) Larsen, T.; Schultz, K.; Furst, E. M. Hydrogel microrheology near the liquid-solid transition. *Korea-Australia Rheol. J.* **2008**, *20*, 165−173.
(66) Winter, H. H.; Chambon, F. Analysis of linear viscoelasticity of a crosslinking polymer at the gel point. *J. Rheol.* **1986**, *30*, 367−382.
(67) Stauffer, D.; Coniglio, A.; Adam, M. Gelation and Critical Phenomena. *Polymer Networks* **1982**, *44*, 103−158.
(68) Corrigan, A. M.; Donald, A. M. Passive microrheology of solvent-induced fibrillar protein networks. *Langmuir* **2009**, *25*, 8599−8605.
(69) Desai, S.; Carberry, B.; Anseth, K. S.; Schultz, K. M. Cell−Material Interactions in Covalent Adaptable Thioester Hydrogels. *ACS Biomater. Sci. Eng.* **2024**, *10*, 5701−5713.
(70) Indana, D.; Agarwal, P.; Bhutani, N.; Chaudhuri, O. Viscoelasticity and adhesion signaling in biomaterials control human pluripotent stem cell morphogenesis in 3D culture. *Adv. Mater.* **2021**, *33*, No. 2101966.

https://doi.org/10.1021/acs.macromol.5c00487
Macromolecules 2025, 58, 3872−3885